UDK 669.14.018.8:57.012.3
Original scientific article/Izvirni znanstveni članek

ISSN 1580-2949
Mater. Tehnol.

COMPOSITION DESIGN OF 316LN AUSTENITIC STAINLESS STEEL FOR LIQUID-HYDROGEN STORAGE BASED ON HIGH-FLUX PREPARATION

OBLIKOVANJE KEMIJSKE SESTAVE AUSTENITNEGA JEKLA VRSTE 316LN ZA SHRANJEVANJE TEKOČEGA DUŠIKA NA OSNOVI PRIPRAVE Z VISOKO UČINKOVITIM TALILOM

Xin Ouyang[1,2], Xuemin Wang[1*], Xinming Hu[2,3], Mengnan Xing[2,3], Chenxi Liu[2,3], Zongxu Pang[2,3]

[1]Collaborative Innovation Center of Steel Technology, University of Science and Technology Beijing, Beijing 100083, PR China
[2]State Key Laboratory of Metal Material for Marine Equipment and Application, Anshan, Liaoning 114009, PR China
[3]Iron and Steel Research Institute of Ansteel Group, Anshan, Liaoning 114009, PR China

Prejem rokopisa – received: 2024-04-24; sprejem za objavo – accepted for publication: 2024-09-06

doi:10.17222/mit.2024.1167

Designing multi-element alloy compositions to achieve target performance was the first step in the development of modern materials, but the traditional trial-and-error experiment seriously restricted the development of new materials due to its low efficiency. In this investigation, the composition design of 316LN austenitic stainless steel for enhanced liquid-hydrogen storage using multi-crucible synchronous metallurgy in a high-flux experiment was proposed. Sixteen groups of as cast austenitic stainless steel samples with different compositions were smelted using high-flux material preparation. Then, through the observation of their microstructures, the chemical composition that best matched the target performance was finally selected. The results show that high-throughput experiments can greatly improve the efficiency of composition design optimization of new stainless steel products. At the same time, this investigation also analyzed the elemental composition of δ-ferrite and the method for effectively controlling the δ-ferrite content. In 316LN stainless steel, Cr and Mo were easily enriched in ferrite grains or grain boundaries, forming Cr and Mo enriched regions. This resulted in a gradient transition of Cr and Mo from the ferrite region to the austenite region, forming galvanic corrosion. In this study, the distribution of Cr, Mo and other elements in 316LN stainless steel was studied by means of a metallographic microscope, electron probe microanalysis, transmission electron microscope and scanning electron microscope. In addition, the relationship between the ferrite content and chemical composition was explored. Finally, it was determined that high-temperature, long-term sensitization treatment is an effective method for controlling the δ-ferrite content.

Keywords: austenitic stainless steel, multi-crucible synchronous metallurgy, δ-ferrite, sensitization heat treatment

Oblikovanje kemijske sestave kovinske zlitine z več legirnimi elelementi in ciljanimi lastnostmi je prva faza razvoja novih modernih materialov. Tradicionalni eksperimentalni pristop *preizkus-napaka-nov preizkus* zelo omejuje napreden razvoj novih materialov zaradi njegove majhne učinkovitosti. V tem članku avtorji opisujejo dizajn kemijske sestave nerjavnega austenitnega jekla vrste 316LN za hitro shranjevanje tekočega dušika. Pri tem so predlagali za izdelavo te vrste jekla uporabo sinhrone metalurgije več talilnih loncev in uporabo visoko učinkovitega talila. Vzorce šestnajstih skupin litega nerjavnega jekla z različno kemijsko sestavo so izdelali v prisotnosti zelo učinkovitega talila. Nato so opazovali mikrostrukturo nastalih litin in na koncu izbrali kemijsko sestavo tiste, ki se je ujemala z najbolj želeno mikrostrukturo in ciljanimi lastnostmi. Rezultati so pokazali, da izvedeni visoko produktivni preizkusi lahko močno izboljšajo učinkovitost optimizacije dizajna novih izdelkov iz nerjavnega jekla. Istočasno so avtorji raziskovali in analizirali povezavo med kemijsko sestavo in vsebnostjo δ-ferita. V nerjavnem jeklu 316LN se feritna kristalna zrna in kristalne meje enostavno (hitro) obogatijo s Cr in Mo. Posledica je nastanek galvanske korozije zaradi postopnega prehoda vsebnosti Cr in Mo s feritnih na austenitna področja. V tem članku so avtorji porazdelitev Cr, Mo in drugih elementov v izdelanih nerjavnih jeklih tipa 316LN študirali s pomočjo svetlobnega mikroskopa, vrstičnega in presevnega elektronskega mikroskopa, elektronskega mikroanalizatorja, in eksperimentalno enačbo za odvisnost med kemijsko sestavo in vsebnostjo delta ferita. Ugotovili so še, da je visoko temperaturna in dolgotrajna senzibilizacijska toplotna obdelava učinkovita metoda za kontrolo vsebnosti δ-ferita.

Ključne besede: austenitno nerjavno jeklo; sinhrona metalurgija v več talilnih loncih; δ-ferit; senzibilizacija toplotne obdelave

1 INTRODUCTION

When developing new materials with specific target properties, the traditional material research used to adopt the empirical trial-and-error method, and explore the best performance of materials by adjusting the sample composition and production process discretely through a small number of experiments. However, this research and development method, which relied heavily on a large number of pilot experiments, was time-consuming and expensive. At the same time, due to a small amount of experimental data, the investigation on the relationship between material composition and performance was not comprehensive and thorough. With the rise of material genome engineering,[1–3] the use of high-throughput experiments, computer performance prediction and other methods to accelerate the development of new materials attracted more and more attention. The high-throughput

*Corresponding author's e-mail:
wxm@mater.ustb.edu.cn (Xuemin Wang)

material preparation method significantly improves the efficiency of material preparation due to its multi-station, automated and parallel characteristics. It can allow a rapid and large-scale synthesis of materials. Compared with the traditional single-sample production mode, its preparation efficiency is significantly improved.[4–5] With the accumulation of experimental data, material database plays an increasingly important role in the process of new material research and design. By screening the database and finding candidate materials closest to the target performance requirements, high-throughput experiments have gradually become a powerful method for obtaining large amounts of high-quality and self-consistent experimental data.

2 EXPERIMENTAL PART

High-flux smelting method for controlling chemical composition is mainly used for the preparation of homogeneous as cast samples with complex alloy compositions, including additive manufacturing, multi-mode casting, multi-crucible synchronous metallurgy, etc. In this study, multi-crucible synchronous metallurgy was used to prepare as cast samples.[6,7] The test process included alloy sample batching, arc melting, grinding and polishing, microstructure observation, rolling, heat treatment and mechanical property inspection. The high-flux alloy preparation system adopted had a 16-station automatic arc melting furnace, as shown in **Figure 1**. For the alloy melting process of this experiment, we adopted a

Figure 1: High-flux material multi-crucible synchronous smelting system: a) high-purity metal block raw materials; b) high-throughput preparation system; c) control interface; d) multi-crucible synchronous metallurgical platform; e) as cast metal ingots with different compositions

Table 1: Chemical composition of a steel ingot prepared in the second round of high-flux preparation (in mass fractions (w/%))

Composition range	C 0.04 - 0.08	Si = 0.75	Mn 1.00 - 2.00	P = 0.03	S = 0.015	Cr 16.00 - 18.00	Ni 11.00 - 13.00	Mo 2.00 - 3.00	Test plan	
B1	0.04	0.4	1.6	0.015	0.005	18	11	2	Scheme 1: investigate the effect of Cr on ferrite content when the content of austenite-forming elements is the lowest	
B2	0.04	0.4	1.6	0.015	0.005	17	11	2		Scheme 2: investigate the effect of Mo on ferrite content when the content of austenite-forming elements is the lowest
B3	0.04	0.4	1.6	0.015	0.005	16	11	2		
B4	0.04	0.4	1.6	0.015	0.005	16	11	3		
B5	0.06	0.4	1.6	0.015	0.005	18	11	2	Scheme 3: investigate the effect of Cr on ferrite content at high C	
B6	0.06	0.4	1.6	0.015	0.005	17	11	2		
B7	0.06	0.4	1.6	0.015	0.005	16	11	2		Scheme 4: investigate the effect of Mo on ferrite content at high C
B8	0.06	0.4	1.6	0.015	0.005	16	11	3		
B9	0.04	0.4	1.6	0.015	0.005	18	13	2	Scheme 5: in the case of high Ni, the effect of Cr on ferrite content is investigated	
B10	0.04	0.4	1.6	0.015	0.005	17	13	2		
B11	0.04	0.4	1.6	0.015	0.005	16	13	2		Scheme 6: investigate the effect of Mo on ferrite content in the case of high Ni
B12	0.04	0.4	1.6	0.015	0.005	16	13	3		
B13	0.06	0.4	1.6	0.015	0.005	18	13	2	Scheme 7: investigate the effect of Cr on ferrite content when the content of austenite-forming elements is the highest	
B14	0.06	0.4	1.6	0.015	0.005	17	13	2		
B15	0.06	0.4	1.6	0.015	0.005	16	13	2		Scheme 8: investigate the effect of Mo on ferrite content when the content of austenite-forming elements is the highest
B16	0.06	0.4	1.6	0.015	0.005	16	13	3		

high-throughput alloy preparation system, which realized a multi-station, automated and efficient operation in all stages of material preparation, thus significantly reducing the average experimental preparation and operation time needed for a sample. For example, the system avoided the cumbersome steps of multiple vacuum pumping of the traditional arc melting method, and successfully overcame the bottleneck of time-consuming material preparation. Compared with the traditional single- or multi-sample preparation methods, the overall efficiency of the high-throughput alloy preparation system is increased by at least 10 times, showing significant advantages in the field of material preparation.

3 RESULTS

According to the literature,[8–9] the ratio of γ-austenite to δ-ferrite was comprehensively affected by γ-austenite forming elements (such as Ni, Mn, N, etc.) and δ-ferrite forming elements (such as Cr, Mo, Si, etc.). The formation of δ-ferrite was mainly sensitive to the segregation of C, Ni, Cr and Mo. Carbon easily forms carbides with chromium, and the element segregation caused by carbides promotes the formation of δ-ferrite. Nickel inhibits the precipitation of δ-ferrite by improving the stability of austenite and reducing the martensitic transformation temperature. When the molybdenum content is high, it increases the tendency of brittle phases such as δ-ferrite to precipitate. In this study, the contents of sensitive elements were adjusted through 16 groups of high-throughput tests to find the target chemical composition with the lowest ferrite content. The test scheme is shown in **Table 1**, and the ferrite measurement results are shown in **Figure 2**.

Results showed that the ferrite content in the metallographic structures of B2, B3 and B7 test ingots was low. The three groups of ingots were heated, rolled and solution heat treated. The ferrite content of the hot-rolled test plates was measured. The observation results for the ferrite content are shown in **Figure 3**. The common feature of the three components was the fact that the contents of Ni, Cr and Mo were controlled according to the middle and lower limits. From the perspective of meeting the mechanical properties, it was

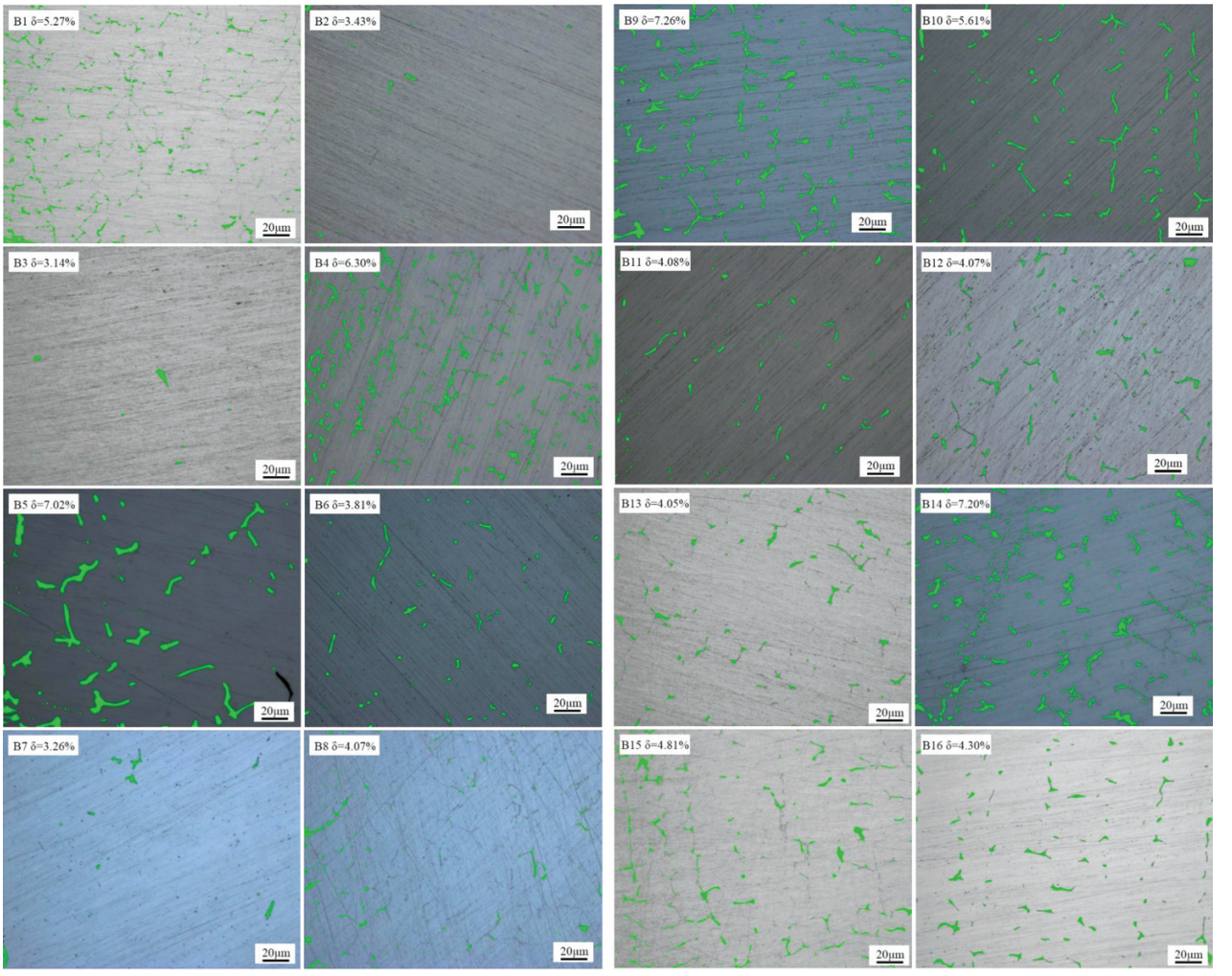

Figure 2: Metallographic photograph of ferrite content of the steel ingot prepared during the second round of high-flux processing

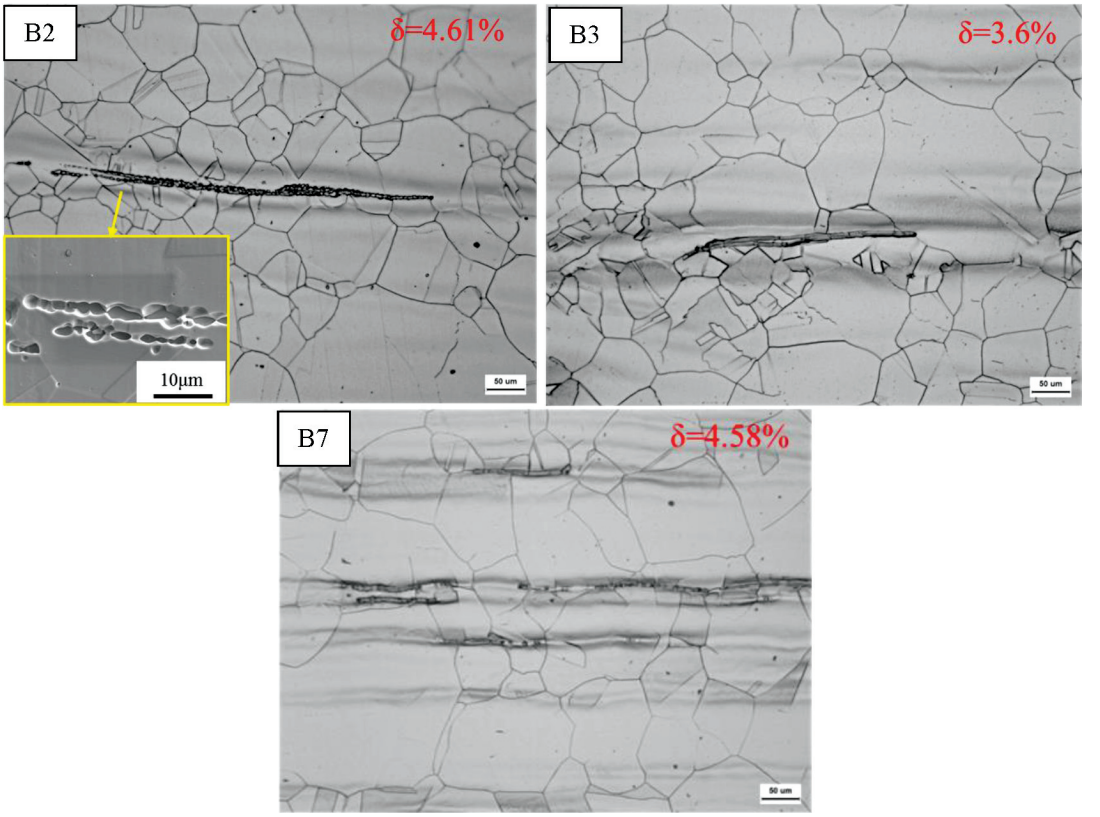

Figure 3: Measurement results for the ferrite content of hot-rolled test plates

recommended to select the chemical composition of the B7 test plate with a high carbon content as the target component. However, with the increase in the carbon content, the ferrite content of the test plate also increased. Other means must be used to optimize the alloy elements so that they achieve a good match between the mechanical properties and microstructure.

4 DISCUSSION

In this study, the stability of ferrite was destroyed with chemical methods to reduce the content of ferrite in austenitic stainless steel.[10] Large ferrite was divided into the granular and unstable state. Due to the particularity of 316LN stainless steel, it can be sensitized at a higher temperature for a long time (about 850 °C). According to the composition characteristics of carbides and ferrites, long-term heat preservation in a high-temperature environment accelerated the precipitation of chromium-enriched ferrites, resulting in $M_{23}C_6$ distributed at the austenite grain boundaries as discontinuous small particles. In addition, carbon atoms quickly dissolve back into austenite at high temperature, so it was easy to destroy the stable structure of original ferrite during subsequent high-temperature annealing or solid solution treatment.[11] In this process, the large ferrite was cut into a lot of granular small pieces that become very unstable due to the re-dissolution of carbon atoms at subsequent high temperatures, which was conducive to the rapid dissolution of ferrite.

Figure 4 shows the microstructure of sample B7 after the sensitization treatment at 850 °C for 4 h. It can be clearly seen from **Figures 4a)** and **4b** that the large strip ferrite in the center after sensitization was divided into granular carbides. $M_{23}C_6$ carbide belongs to the face-centered-cubic (FCC) structure, so its diffraction pattern shows the characteristics of this structure. According to the observation results for the transmission structure and diffraction spots, the diffraction ring or spot group of carbides precipitated at the grain boundaries was centered around the optical axis of the transmission electron microscope, showing a circular or nearly circular distribution; diffraction spots showed a central symmetrical pattern, proving that the carbide was mainly composed of $M_{23}C_6$.[12]

Figure 5 shows the ferrite content and morphology of sample B7 before and after sensitization and solid solution. It shows that the microstructure etched with potassium hydroxide electrolysis does not only clearly show the outline of grain boundary, but also the residual δ-ferrite. On **Figure 5a**, we can clearly see that the color of the δ-ferrite region is black, which is due to the significant damage of the passive film in this region. There were two main reasons for this failure: first, because of its low Perner force and stacking fault energy, austenite experienced slip of edge dislocation relatively easily,

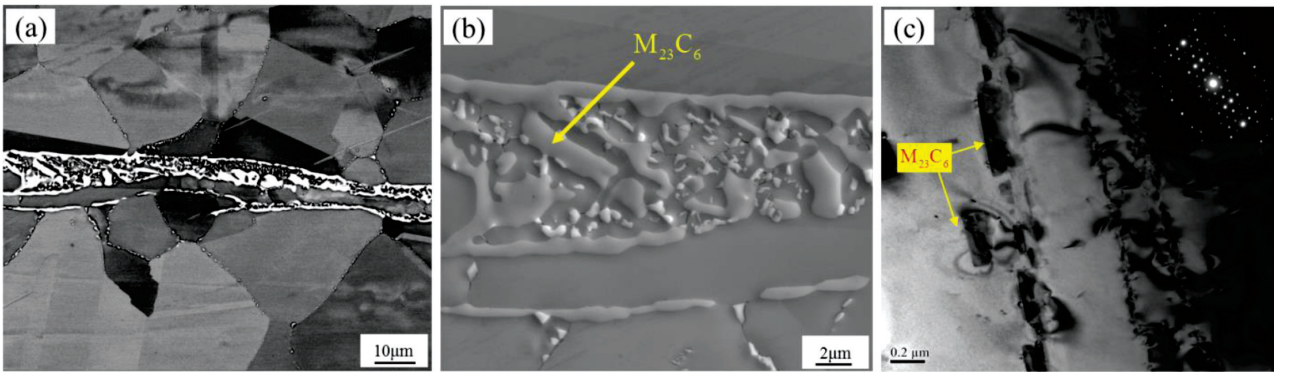

Figure 4: Sensitized microstructure of 316LN stainless steel: a) metallographic photos of macromorphology; b) partially enlarged scanning electron microscope photograph; c) TEM morphology and diffraction pattern

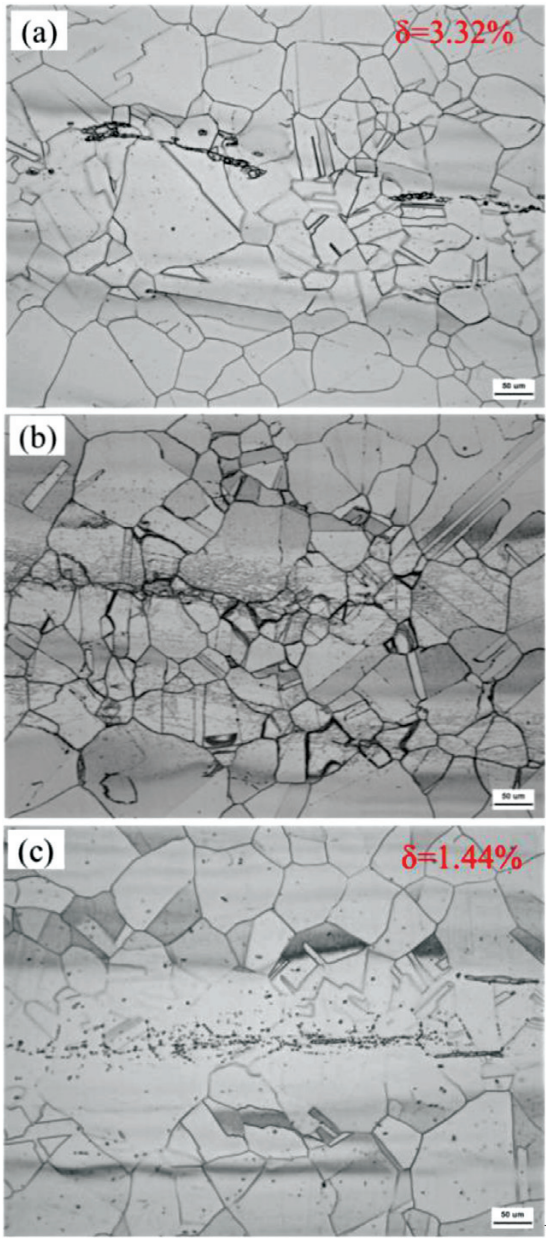

Figure 5: Ferrite morphology and content of 316LN stainless steel before and after sensitization: a) rolled state; b) 850 °C × 4 h sensitized state; c) 1060 °C × 1 h solid solution

while δ-ferrite was more prone to cross-slip of screw dislocations due to its higher stacking fault energy. This led to the inhomogeneity of the passive film on the surface of the material, and then affected the stability of the passive film so that the dissolution rate of the passive film in the δ-ferrite region was much higher than that of austenite.[13]Secondly, during the hot rolling process, the flattened δ-ferrite concentrated a large number of high-density dislocations, making its energy higher than that of the austenite matrix. This led to a difference in the electrochemical properties between the austenite matrix and the residual δ-ferrite, forming a corrosion micro cell, in which δ-ferrite was used as the anode and the austenite matrix was used as the cathode; as a result, δ-ferrite was more vulnerable to corrosion, resulting in a black appearance.[14]

It can be seen from **Figure 5** that the ferrite content decreases by about 50 % after the sensitization and solid solution processes, meeting the requirements of ≤3 %, but there is still a gap to achieve a reduction to ≤1 %. The main reason for this is the fact that the sensitization treatment does not only destroy ferrite, but also promotes the formation of carbides. During the sensitization process, the formation of carbides was accompanied by a local high enrichment of Cr and Mo, resulting in the segregation of alloy elements in the matrix. During the subsequent solution heat treatment, these previously formed carbides disintegrated, and the elements in them were re-dissolved into the matrix. However, due to the local high concentration of Cr and Mo in the sensitization stage, their diffusion dissolution during the solid solution heat treatment was limited.

Figure 6 shows the microstructure of sample B7 after sensitization treatment and solid solution treatment at 1060 °C. It can be seen from **Figure 6a** that carbides were eliminated after the solution treatment, but there was still a certain amount of carbides in the local δ-ferrite areas. As shown in **Figure 6b,** after corrosion, it was obvious that a δ/γ grain boundary with a width of 1.5–2 μm formed a corrosion-dissolved structure. The corrosion resistance of the δ-ferrite, austenite and two-phase interface was different, leading to the formation of gal-

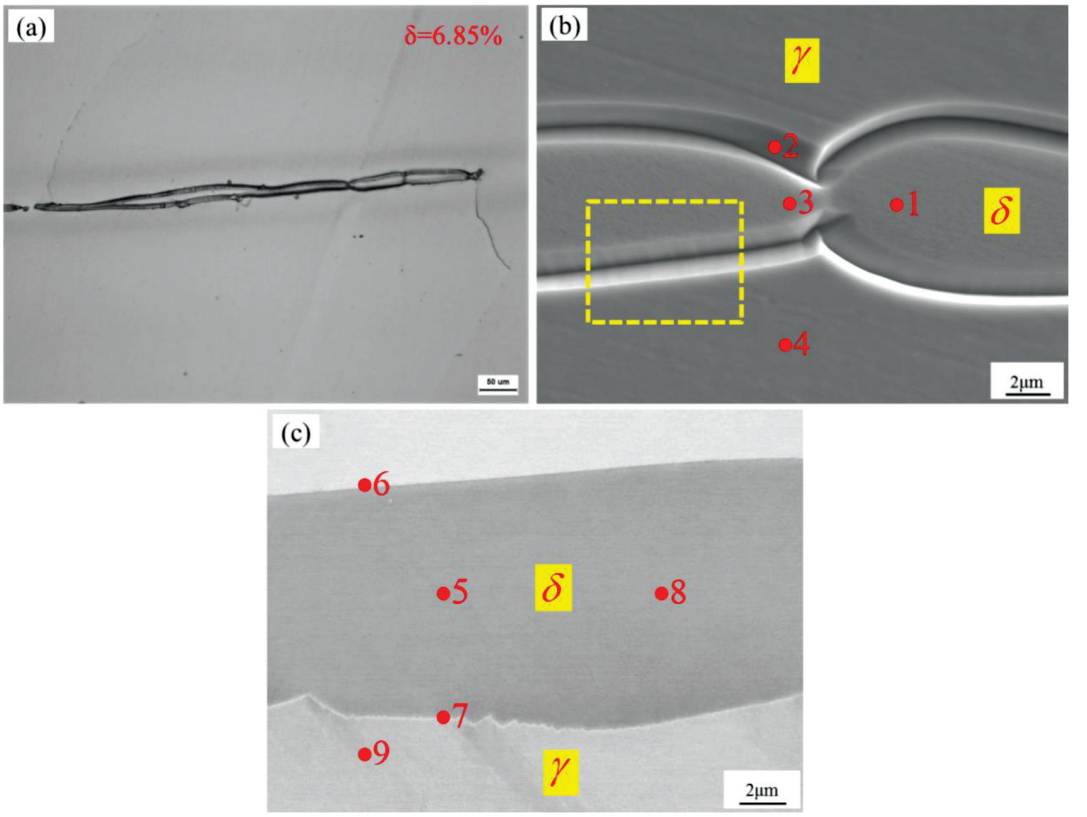

Figure 6: Microstructure of 316LN stainless steel after sensitization and solid solution: a) metallographic structure; b) metallographic structure (EPMA); c) electropolished state (EPMA)

vanic corrosion. The content of alloying elements in the δ-ferrite structure was high, and the electrode potential was high. The content of alloying elements in the austenite structure was low, and the electrode potential was high. Due to the unequal electrode potentials of metals, a corrosion battery was formed, causing the galvanic current to flow from the high potential area to the low potential area, thus increasing the metal dissolution rate at the two-phase interface, and resulting in local corrosion.[15]

In order to explain the cause of galvanic corrosion, the sample was electropolished, as shown in **Figure 6c**, to retain ferrite and all the surrounding structures. Then the compositions of the polished original structure and the corroded structure were analyzed, as shown in **Table 2**. During electrolytic corrosion, the electrode metal rod with a high potential was used as the anode, and its dissolution rate was faster. Stainless steel was used as the cathode, and its dissolution rate was slower, while the surface was protected by the anode.[16,17] In addition, the degree of galvanic corrosion was reduced by adjusting the area ratio of anode and cathode and reducing the dielectric conductivity with a 10-% KOH aqueous solution so that the structure of the transition region of the two-phase interface could be retained. It can be seen from the table that in the microstructure of metallographic corrosion, the δ-ferrite region contained high amounts of Cr and Mo, with maximums of 20.59 *w*/% and 5.18 *w*/%, respectively. This was due to the ferrite with high Cr and Mo amounts. These amounts of Cr and Mo gradually decreased from the center of ferrite to the austenite zone, and the amounts of Cr and Mo in the austenite around ferrite were about 18 % and 2.9 %, respectively. The amount of Mo was also higher than that in typical 316LN, indicating that the composition around δ-ferrite had reached an equilibrium state.

Table 2: Analysis of energy spectra from **Figure 6** (in mass fractions (*w*/%))

No	Cr	Mo	Ni	Si	Mn
1	**20.59**	**5.18**	**9.35**	**0.56**	**1.77**
2	17.81	2.90	12.23	0.80	1.73
3	**20.25**	**4.27**	**9.42**	**0.70**	**2.17**
4	16.38	2.87	12.47	0.62	2.43
5	**20.36**	**4.78**	**9.48**	**0.57**	**1.89**
6	17.64	2.93	12.12	0.57	2.56
7	17.75	3.84	10.13	0.47	1.59
8	**20.67**	**4.58**	**9.55**	**0.51**	**2.41**
9	17.10	2.24	12.92	0.53	1.82

5 CONCLUSIONS

1. In this study, the composition optimization design of 316LN austenitic stainless steel for liquid-hydrogen storage and transportation equipment was advanced with high-throughput experiments, and comprehensive design

efficiency was increased by more than 20 times. Stainless steel ingots differing by a single component were prepared in large quantities using the multi-crucible synchronous metallurgy method, which was at least 10 times faster than the traditional single/few sample preparation. This work proved the feasibility of doubling the speed of material research and development with low cost proposed by the Materials Genome Initiative, where the high-throughput experimental method can become an effective general strategy to accelerate the optimization design of material composition.

2. Reducing the Creq/Nieq ratio within the composition range, especially controlling the amounts of Cr and Mo, allowed us to fundamentally reduce the formation of ferrite and control its content. When the composition was fixed, the ferrite content had to be controlled from two aspects: sensitization treatment and solution treatment.

3. Under existing process conditions, the method of high-temperature sensitization and solid solution treatment was more effective in reducing ferrite, meeting the requirement of δ-ferrite = 3 %. However, it could not achieve δ-ferrite = 1 % or completely eliminate it. A large number of carbides were generated during the sensitization heat treatment; however, although the carbides could disintegrate ferrite at the same time, the enriched Cr and Mo were difficult to diffuse during the subsequent solid solution heat treatment. As a result, a smooth transition of the concentration gradients of Cr and Mo was easily formed, thus causing galvanic corrosion.

Acknowledgment

The authors acknowledge the support of the Fundamental Research Business Funds for Central Universities (FRF-BD-22-02).

6 REFERENCES

[1] Z. Wang, M. Wang, Q. L. Yong, et al., Materials Informatics and its Application in Materials Research, Materials China, 36 (**2017**) 2, 132–140, doi:10.7502/j.issn.1674-3962.2017.02.08

[2] Y. Z. Lv, Z. X. Qin, X. Lu, Current Research Status of High-Throughput Development of Amorphous Alloys, Materials Reports A: Review Papers, 31 (**2017**) 9, 112, doi:10.11896/j.issn.1005-023X.2017.017.016

[3] Y. H. Liu, Z. H. Hu, Z. G. Su, et al., Current Status of High Throughput Experimental Technology and its Application in Research of Precious Metals, Science China Technological Sciences, 62 (**2019**) 4, 521–545, doi:10.3969/j.issn.1004-0676.2018.z1.014

[4] W. Jiong, et al., Machine learning assisted high-throughput experiments to accelerate hard high entropy alloys, Progress in Materials in China, 39 (**2020**) 4, 269–277, doi:CNKI:SUN:XJKB.0.2020-04-004

[5] X. Wen, F. Zhang, et al., Second Phase Strengthening in High-Entropy Alloys, Materials China, 38 (**2019**) 3, 53, doi:10.7502/j.issn.1674-3962.2019.03.06

[6] M. Bao, J. Qiao, Research Progress of Hexagonal Close-Packed High-Entropy Alloys, Materials China, 397 (**2018**) 4, 314–319, doi:10.7502/j.issn.1674-3962.2018.04.03

[7] C. Li, Y. Hou, et al., Diffusion Dynamic Analysis on Selective Laser Melting Process of Fe/Ni Powder, Materials Review, 34 (2020) Z1, 117–130

[8] J. Li, Y. Zhuang, W. Yin, Formation and control of ferrite in 316H stainless steel, Steel, 57 (**2022**) 11, 123–130, doi:10.13228/j.boyuan.issn0449-749x.20220293

[9] S. Aras, R. Ertan, Studying the strength of dissimilar joints of AISI 430 and 301 stainless steel welded at different welding parameters, Mater. Tehnol., 58 (**2024**) 2, 123–130, doi:10.17222/ mit.2023.1054

[10] Z. Pang, et al., Residual in S31609 austenitic stainless steel δ corrosion behavior of ferrite, China Metallurgical, 31 (**2021**) 3, 59–65, doi:10.13228/j.boyuan.issn1006-9356.20200451

[11] Y. S. Sato, H. Kokawa, Preferential precipitation site of sigma phase in duplex stainless steel weld metal, Scripta Materialia, 40 (**1999**) 6, 659, doi:10.1016/S1359-6462(98)00483-7

[12] X. Huangfu, X. Wang, W. Wang, Study on characteristics of residual ferrite in solidification structure of austenitic stainless steel, Iron and Steel, 47 (**2012**) 4, 74, doi:10.13228/j.boyuan.issn0449-749x.2012.04.006

[13] H. Dong, Comparative study on microstructure evolution of austenite and ferrite during cyclic deformation, Dalian: Dalian University of Technology, 2020, doi:10.26991/d.cnki.gdllu.2019.001550

[14] J. Wang, Calculation of electronic work function and its application in the study of electrochemical problems on the surface of materials, Hefei: University of Science and Technology of China, 2016

[15] Z. Peng, L. Cai, F. Peng, et al., P92 steel δ effect of ferrite on the composition and volume fraction of precipitates aged at 700 and 750 °C, Acta Metalica Sinica, 48 (**2012**) 11, 37, doi:CNKI:SUN:JSXB.0.2012-11-007

[16] B. Schlüter, G. Barkleit, F. Schneider, et al., Analysis of intergranular corrosion attack of stainless steels by means of atomic force microscopy and optical microscopy. Part2: Influence of impurity content, Mater. Corros., 51 (**2015**) 2, 115, doi:10.1002/(SICI)1521-4176(200002)51:2<115::AID-MACO115>3.0.CO;2-N

[17] G. Barkleit, F. Schneider, et al., Analysis of intergranular corrosion attack of stainless steels by means of atomic force microscopy and optical microscopy. Part 1: Influence of treatment, Mater. Corros., 51 (**2000**) 2, 109, doi:10.1002/(SICI)1521-4176(200002)51:2<109::AID-MACO109>3.0.CO;2-B